
Learning the Language of NMR: Structure Elucidation from NMR spectra using Transformer Models

Anonymous Author(s)

Affiliation

Address

email

Abstract

1 The application of machine learning models in chemistry has made remarkable
2 strides in recent years. Even though there is considerable interest in automating
3 common procedure in analytical chemistry using machine learning, very few
4 models have been adopted into everyday use. Among the analytical instruments
5 available to chemists, Nuclear Magnetic Resonance (NMR) spectroscopy is one of
6 the most important, offering insights into molecular structure unobtainable with
7 other methods. However, most processing and analysis of NMR spectra is still
8 performed manually, making the task tedious and time consuming especially for
9 large quantities of spectra. We present a transformer-based machine learning model
10 capable of predicting the molecular structure directly from the NMR spectrum. Our
11 model is pretrained on synthetic NMR spectra, achieving a top-1 accuracy of 67.0%
12 when predicting the structure from both the ^1H and ^{13}C spectrum. Additionally, we
13 train a model which, given a spectrum and a set of likely compounds, selects the
14 structure corresponding to the spectrum. This model achieves a top-1 accuracy of
15 98.28% when trained on both ^1H and ^{13}C spectra in selecting the correct structure.

16 1 Introduction

17 Nuclear magnetic resonance (NMR) spectroscopy is widely considered the most crucial tool in
18 determining the structure of molecules [1]. Unlike other techniques such as infrared (IR) spectroscopy
19 or mass spectroscopy (MS), NMR provides comprehensive and human-interpretable information
20 about the molecule. It reveals details such as the number of NMR-active nuclei, the functional group
21 to which a peak belongs, and, for some nuclei, information about its surrounding environment [2].
22 Typically the spectra of multiple NMR-active nuclei are used to definitely assign the structure. Most
23 commonly, an ^1H NMR and a ^{13}C NMR are used for this purpose. In the literature, the combination
24 of these two spectra has become the *de facto* proof that a compound has been synthesised [3].
25 Consequently, NMR spectroscopy has risen to prominence as the preferred analytical instrument in
26 standard chemical laboratories.

27 Nevertheless, analyzing NMR spectra is not straightforward. Although there are various software
28 tools available to assist chemists in this process, the majority of spectra are still processed manually.
29 As a result, the analysis of NMR spectra, particularly in large quantities, becomes a time-consuming
30 and tedious undertaking [4].

31 The increasing availability of computational power has ushered in a new era of statistical methods:
32 machine learning and deep learning. These approaches have revolutionized fields such as image
33 classification and language modeling by addressing previously unsolvable problems [5, 6]. In the
34 realm of chemistry, machine learning, and particularly language modeling, has emerged as a highly

35 promising tool. Such models have diverse applications, spanning from predicting retrosynthetic
36 routes over designing new drug candidates to assisting in the automation of experiments [7, 8, 9].

37 In addition to changes brought about by machine learning, chemistry is experiencing a paradigm
38 shift due to the growing prominence of robotics and automation in laboratories [10, 11]. Advances in
39 both fields have carried over into chemistry, enabling fully automated high-throughput experimental
40 campaigns that generate vast volumes of data previously inaccessible. By operating at nanomolar
41 scales, these techniques can conduct hundreds to thousands of reactions per day [12, 13, 14, 15].
42 However, one crucial step remains a limitation: the analysis of the reaction products.

43 Current high-throughput approaches are predominantly restricted to a limited number of reagents and
44 reactants, largely due to their heavy reliance on high-performance liquid chromatography (HPLC)
45 systems. Each reactant and product necessitates a separate calibration curve, imposing limitations on
46 the chemical space that can be explored [16, 17]. Despite the automation of most physical handling
47 steps, the analysis of the resulting data still predominantly relies on manual labor, demanding weeks to
48 months of tedious work. Among these tasks, the analysis of NMR data obtained from high-throughput
49 experiments can be particularly burdensome.

50 Even though the analysis of NMR spectra obtained from high-throughput experiments remains time
51 consuming, advances have been made to alleviate the burden to some extent. Commercial NMR
52 software offers options to automate peak picking, integration and multiplet assignment of the spectra
53 [18, 19]. However, automatically determining a structure from the spectra without strong prior
54 knowledge is currently not feasible. Approaches addressing this task using machine learning have so
55 far been limited in the sense that they either limit the number of elements, the heavy atom count (all
56 atoms other than hydrogen) or solely rely on one type of spectrum (e.g. ^{13}C) [20, 21, 22, 23, 24].

57 To close the loop between automated high throughput experiments and NMR spectroscopy, an
58 automated NMR structure elucidation workflow is required. Here we propose to utilise language
59 models trained on NMR spectra to directly predict the structure. We achieve a top-1 accuracy in
60 predicting the correct molecular structure from simulated ^1H and ^{13}C NMR spectra of 67.0%. If the
61 language model is provided with additional information such as the reagents and expected products of
62 a reaction, the model is able to identify the correct structure in 98.28% of cases from the combination
63 of both the ^1H and ^{13}C NMR spectrum.

64 **2 Results and Discussion**

65 We focus on two primary tasks. The first one involves predicting the molecular structure directly
66 from the ^1H spectrum, ^{13}C spectrum, or the combination of both spectra. The second one focuses on
67 exploring the effect of adding additional context to the NMR spectrum. This second task corresponds
68 to a typical high-throughput scenario, where chemists are aware of the reaction that was conducted
69 and, consequently, the potential molecules present in the spectrum. We task the model to match the
70 correct molecule to a given spectrum.

71 **2.1 Data**

72 As the number of publicly available experimental NMR spectra is limited, we simulate a large
73 training set using MestreNova [18]. We sample reactions from the Pistachio dataset [25] and simulate
74 NMR spectra for both the reactants and products. In contrast to previous work, we do not exclude
75 stereoisomers or restrict the heavy atom count drastically, opting for a range of 5 to 35, with an
76 average heavy atom count of 22.7. We limit the elements to the ones most commonly found in organic
77 chemistry, excluding molecules with elements other than carbon, hydrogen, oxygen, nitrogen, sulfur,
78 phosphorous and the halogens. In total we generate 1.94 million ^1H and ^{19}F decoupled ^{13}C NMR
79 spectra as well as 1.10 million ^1H NMR spectra. Further details on the molecules can be found in
80 Appendix A.1.

81 Instead of utilizing the raw ^1H NMR spectrum, as demonstrated previously by Huang et al. [20], we
82 opt for a processed version of the spectrum. There are two main reasons behind this choice. Firstly,
83 if starting from the raw vector, the model would need to learn concepts such as peak picking, peak
84 integration, and multiplet assignment. Our approach reduces the learning demand on the model
85 by preprocessing the spectra using MestreNova. Secondly, the wide availability of such processed
86 experimental NMR spectra in papers and patents presents a potential avenue for validating our models

87 on experimental data. Further information on the exact simulation details can be found in Appendix
88 A.1.

89 2.2 Model

90 In this study, we adopt a sequence-to-sequence encoder-decoder transformer architecture, build-
91 ing upon the formulation utilized in our previous investigation of IR spectra [26]. More detailed
92 information can be found in Appendix A.2.

93 As discussed above, we employ the processed NMR representation of a spectrum instead of a vector.
94 For the ^1H NMR this takes the form of a string containing the position of the peak in ppm, the
95 multiplet type ('s', 'd', 't', etc.), and the integration of the peak (i.e. the number of hydrogen atoms).
96 All ^1H values are rounded to the nearest second decimal. On the other hand, ^{13}C NMR spectra are
97 presented to the model as a simple list of peaks. All values in ppm are rounded to the nearest first
98 decimal. Examples are illustrated in Figure 1. A detailed account of how NMR spectra are processed
99 can be found in Appendix A.3.

100 All molecules are presented to the model as presented to the model as Simplified molecular-input
101 line-entry system (SMILES) [27, 28].

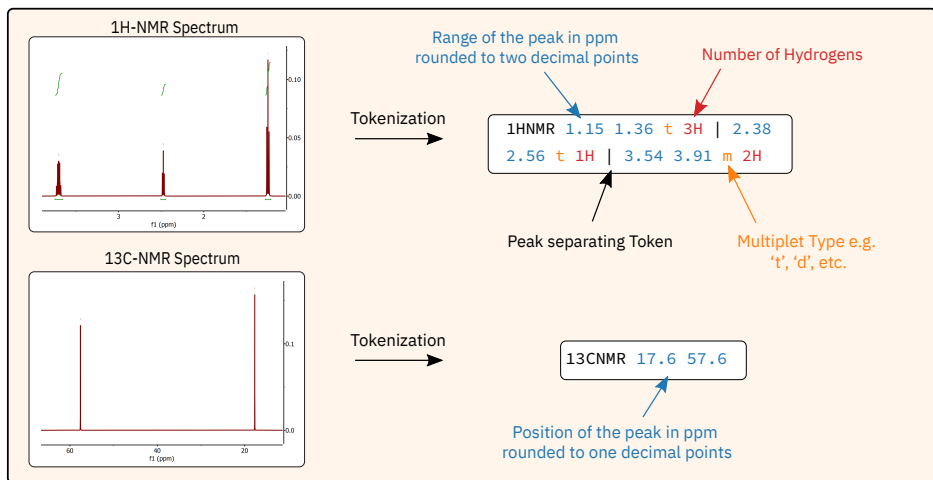


Figure 1: Summary of the tokenization process for NMR spectra. Top: Tokenization of an ^1H NMR spectrum following the Range representation. Bottom: Tokenization of a ^{13}C NMR spectrum.

102 2.3 Structure Prediction from NMR spectra

103 In the following we focus on predicting the molecular structure directly from the NMR spectrum. We
104 assess three different scenarios: Predicting the structure solely from the ^1H NMR spectrum, solely
105 from the ^{13}C NMR spectrum, and from the combined ^1H and ^{13}C NMR spectra.

106 2.3.1 Model optimisation

107 To explore the consequences of various data preparation methods, we examine the effects of supple-
108 menting the model with the chemical formula alongside the spectra, altering the formatting of ^1H
109 NMR peaks, and investigate the effect of a shared or separate token space between the ^1H and ^{13}C
110 NMR peaks. We train 13 models to assess the impact of these changes and evaluate the performance
111 of the trained models based on the top-1, top-5, and top-10 accuracy metrics. These metrics indicate
112 the percentage of cases in which the predicted structure matches the target structure within the first,
113 first five, and first ten predictions, respectively. Molecules are defined as matching if their canonical
114 SMILES are identical. The results of these experiments can be found in Table 1. In the following, we
115 delve deeper into the different data preparation methods and their respective effects.

116 We trained a model for all the three scenarios (solely ^1H or ^{13}C and combined ^1H and ^{13}C) with and
117 without the chemical formula. We observe an increase in performance of $\sim 8\text{--}14\%$ in performance for

Table 1: Summary of experiments on simulated data and associated metrics.

	Formula	Format*	Tokens [†]	Top-1%	Top-5%	Top-10%
¹ H NMR	✗	Center	N/A	38.29%	54.67%	58.43%
	✓	Center	N/A	53.34%	71.71%	75.09%
	✓	Adaptive	N/A	53.39%	71.84%	75.23%
	✓	Range	N/A	55.32%	73.59%	76.74%
¹ H NMR (Augmented)	✓	Range	N/A	51.58%	70.52%	73.94%
¹ H NMR (Ensemble)	✓	Range	N/A	57.99%	76.65%	80.04%
¹³ C NMR	✗	N/A	N/A	37.21%	53.98%	57.45%
	✓	N/A	N/A	51.37%	70.74%	74.32%
¹³ C NMR (Augmented)	✓	N/A	N/A	49.02%	69.05%	72.90%
¹³ C NMR (Ensemble)	✓	N/A	N/A	53.91%	73.45%	77.72%
¹ H+ ¹³ C NMR	✗	Range	Separate	56.88%	73.91%	76.89%
	✓	Range	Separate	64.78%	81.74%	84.43%
	✓	Range	Shared	65.05%	82.07%	84.70%
¹ H+ ¹³ C NMR (Augmented)	✓	Range	Shared	62.35%	80.15%	82.93%
¹ H+ ¹³ C NMR (Ensemble)	✓	Range	Shared	66.99%	84.09%	86.59%

* The format used to represent the position of the ¹H NMR peaks

Center: Center of the peak

Range: Minimum and maximum ppm of the peak

Adaptive: If the range is larger than 0.15 ppm use the range format otherwise center format

[†] Whether the token space of the ¹H and ¹³C NMR spectrum is shared or separate

118 all three models when including the formula. Adding the chemical formula constrains the chemical
 119 space that the model explores. This transforms the task from predicting the structure based solely on
 120 the spectrum to generating a set of isomers from the chemical formula and matching the best one to
 121 the spectrum. Consequently, we include the formula in all subsequent experiments. Experimentally
 122 the chemical formula is easily obtained via Liquid Chromatography – Mass Spectrometry (LC–MS).
 123 The integration of LC–MS into high-throughput workflows is common and as such this data would
 124 typically be obtained alongside the NMR spectra.

125 Another point of interest is the format in which ¹H NMR peaks are presented to the model. In the
 126 literature, two formats are commonly used to describe ¹H NMR peaks. For smaller, narrower peaks,
 127 the center of the peak is typically used. Conversely, for larger, broader peaks, the peak is described as
 128 a range by indicating the minimum and maximum values at which the peak begins and ends. Here,
 129 we investigate three cases: (1) providing the model only with the center of the peak, (2) using a range
 130 by specifying the start and end values of each peak, and (3) employing an adaptive approach inspired
 131 by the format found in the literature with thinner peaks using the center and broader peaks the range
 132 representation. We define broad peaks as those with a width greater than 0.15 ppm. The results are
 133 presented in Table 1 within the ¹H NMR section. We find that the range representation yields the
 134 best performance, likely due to the additional information on the width of the peak. Therefore, for all
 135 subsequent experiments involving ¹H NMR spectra, we utilize the range representation.

136 Next, we shift our focus to the combination of ¹H and ¹³C spectra. To assign a structure from NMR
 137 spectra, it is common practice to rely on both the ¹H and ¹³C spectra, as opposed to analysing a single
 138 spectrum on its own. In these experiments, we investigate the impact of providing the model with both
 139 the ¹H and ¹³C NMR spectra. Following our earlier experiments we reuse the best representations for
 140 ¹H spectra and concatenate it with the ¹³C spectrum. More detailed information regarding the data
 141 format utilized to feed the model can be found in Appendix A.3. Additionally, we examine whether
 142 the model performs better when the tokens representing the position of the peaks fall into a shared
 143 space or a separate one. This is achieved by dividing the position of the ¹³C NMR peaks by 10 causing
 144 a significant overlap in tokens describing the position of peaks between the two modalities. The

145 advantage of sharing tokens is a decreased vocabulary size. However, when the tokens are shared the
146 model has to learn to differentiate between ^1H and ^{13}C NMR tokens. The results, presented in Table
147 1 under the $^1\text{H}+^{13}\text{C}$ NMR section, demonstrate that the shared tokenization scheme outperforms the
148 separate one by $\sim 0.25\%$.

149 To enhance the models' performance and promote generalization, we augment the training data.
150 Specifically, we utilize jitter augmentation with a range of 0.5 ppm, as outlined in Appendix A.4.
151 This augmentation approach generates two augmented spectra for each original spectrum. When
152 training the models on the combined augmented and original spectra, we observe a noticeable decline
153 in performance across all scenarios (^1H , ^{13}C , and the combined ^1H and ^{13}C). We hypothesize that
154 this is caused by the reliance of the models on the high homogeneity of the data, its consistency in
155 peak position and width, and the lack of noise. Introducing noise through augmentation disrupts the
156 learning process and results in decreased performance on the simulated test set. However, should
157 the models be evaluated on experimental spectra, which naturally contain noise, we expect that the
158 augmented models would likely perform better.

159 Ensembling was used to further increase the performance of the models. We used an ensemble of the
160 five best performing checkpoints for each model trained on non-augmented data. Across the three
161 scenarios this increases performance on average by $\sim 2.4\%$. Results of the best performing models
162 can be seen in Table 1. Ultimately, our final top-1 accuracy reaches 58.0% for ^1H NMR, 53.9% for
163 ^{13}C NMR, and 67.0% for the combined ^1H and ^{13}C NMR spectra.

164 2.3.2 Model Analysis

165 In the following we analyse the performance of the model across the three tasks. We use the best
166 ensembled model from above and evaluate how the performance of the model changes with respect
167 to the heavy atom count and in relation to the presence of specific functional groups. In addition,
168 we also demonstrate that even if the model makes mistakes, most predicted molecules are relatively
169 similar to the ground truth by evaluating the Tanimoto similarity of all predicted molecules[29].

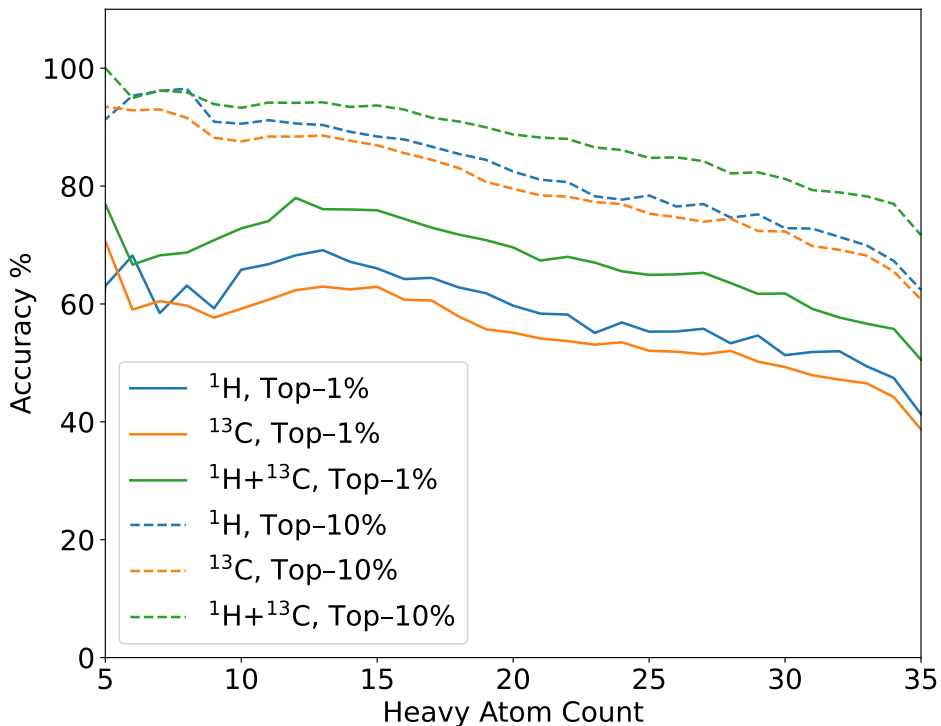


Figure 2: Heavy atom count vs accuracy. Results for ^1H spectra are shown in blue, for ^{13}C in orange and in green for the combination of both.

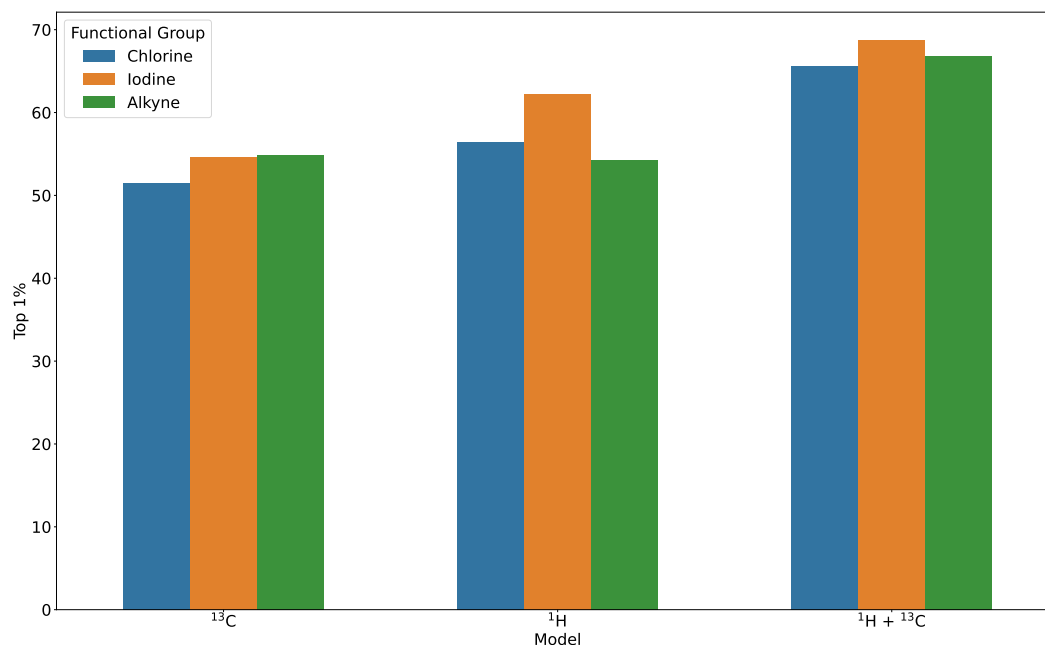


Figure 3: The models ability to correctly predict the molecular structure plotted against the presence of certain functional groups: a) ^1H NMR, b) ^{13}C NMR, c) $^1\text{H} + ^{13}\text{C}$ NMR.

170 Heavy Atom count

171 In order to assess the model's performance, we evaluate its accuracy in relation to the heavy atom
 172 count. Figure 2 shows a negative correlation between the heavy atom count and the model's accuracy.
 173 The model trained on both ^1H and ^{13}C spectra outperforms the models trained on a sole spectrum,
 174 highlighting the complementary information that can be extracted from both types of spectra. As
 175 expected, the ^1H model demonstrates better performance compared to the ^{13}C model, albeit by a
 176 relatively small margin of $\sim 5\%$. The relatively high variability in performance for molecules with a
 177 heavy atom count ranging from 5 to 10 can be attributed to the limited training data available in this
 178 particular range, comprising only around 2.5% of the total training dataset.

179 The negative correlation of the model's performance with the heavy atom count can be attributed to
 180 two factors. Firstly, as the heavy atom count increases, molecules tend to become more complex,
 181 resulting in longer SMILES strings. Since the model generates predictions autoregressively, even
 182 a single incorrect token prediction can lead to a significantly different structure. This sensitivity to
 183 errors becomes more pronounced with an increase in the complexity of the molecules. Secondly, as
 184 the heavy atom count rises, the chemical space expands exponentially, giving rise to a greater number
 185 of potential isomers that the model must differentiate, making the prediction more challenging.

186 Functional Group to Structure

187 We analyse the model's ability to generate the correct structure depending on the presence of certain
 188 functional groups by calculating the top- n metrics for subsets containing a specific functional group
 189 in the test set. The scores are shown for each of the selected functional groups in Figure 3. The
 190 functional group definitions used and full performance across all evaluated functional groups can be
 191 found in Appendix B and C respectively. As with the heavy atom count, the model trained on the
 192 combined spectra outperforms both models trained on a sole spectrum, demonstrating the synergy
 193 that can be obtained by using both.

194 When comparing between the model trained on ^1H and ^{13}C spectra, the ^1H NMR model's performance
 195 is notably higher when predicting molecules containing halogens. This divergence can be attributed
 196 to the fundamental differences between the two modalities. While ^{13}C NMR offers some insight
 197 into the presence of halogens, ^1H NMR spectra provide substantially more information, enabling
 198 conclusions to be drawn regarding the presence and even quantity of halogens on adjacent atoms.

199 Conversely, we find that the ^1H NMR model performs worse compared to the ^{13}C NMR model when
200 predicting molecules containing alkynes. This can be attributed to two factors. Firstly, carbon NMR
201 alkyne peaks are relatively distinctive and easily identifiable. Secondly, in many cases, there are
202 simply no hydrogen atoms directly attached to the alkynes. As a result, alkynes become a potential
203 blind spot for ^1H NMR.

204 When both ^1H and ^{13}C NMR spectra are provided to the model, we observe an improvement for
205 all functional groups. This is especially apparent for both halogens and alkynes compared to the
206 individual models. In fact, these functional groups now perform above average in the combined model.
207 This highlights the the model's capacity to effectively utilize and integrate information from both
208 modalities, thereby harnessing the complementary strengths of the two types of spectra enhancing its
209 predictive capabilities.

210 Similarity

211 We compute the Tanimoto similarity [29] to the ground truth for all predicted molecules using Morgan
212 fingerprints with a radius of 2 and a bit vector size of 1024 [30]. The average Tanimoto similarity is
213 0.534, 0.537, and 0.553 when the prediction relies on ^1H NMR, ^{13}C NMR, and combined spectra,
214 respectively. Examples of molecules predicted by the combined model are shown in Figure 4. Even
215 when the model makes incorrect predictions, most of them still exhibit a high degree of similarity to
216 the ground truth. The similarity distribution for all three models can be found in Appendix D.

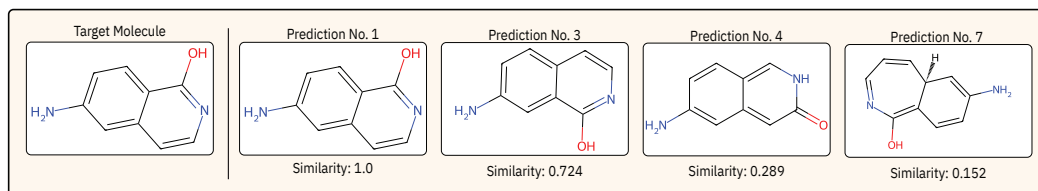


Figure 4: Four predictions of the model trained on the combined data. Illustrated are the target molecule on the left and four predictions on the right, including their rank and similarity to the target molecule.

217 2.4 NMR Matching

218 In this task, our objective is to evaluate the model's ability to accurately match the correct structure
219 to an NMR spectrum based on a set of potential molecules and a spectrum. In practical terms, this
220 task resembles a situation in which, after a reaction has been completed and NMR spectra have been
221 obtained for each fraction, these fractions must be assigned to a potential molecule. For this task,
222 we train models on ^1H , ^{13}C , and their combination. We compare these models to a baseline which
223 randomly picks a molecule from the set.

224 We provide the model with a set of molecules along with an NMR spectrum. The input of the model
225 consists of the SMILES of the potential molecules separated by "." and the spectrum in the optimal
226 data format as developed above. With this input, the model is tasked to either generate the SMILES
227 of the correctly matching molecule or, if no molecule in the set matches the spectrum, a non matching
228 token.

229 We develop two methods to generate the input sets. Firstly, a reaction dataset in which we provide the
230 model with both the reagents and products of a reaction and either a matching or not matching NMR
231 spectrum. Secondly, a dataset consisting of molecules randomly picked from all molecules present in
232 Pistachio. We vary the number of molecules from two to seven to evaluate the models performance
233 as the size of the set increases.

234 The performance of the models is evaluated on the two test sets sampled using the methods above
235 (reaction set (rxn), molecule set (mol)). We measure the overall performance of the model using the
236 top-1 accuracy metrics. Top-1 Accuracy is an appropriate metric in this case as the matching and
237 non-matching set are balanced. Results of the experiments can be found in Table 2. Table 2 shows
238 that the random baseline achieves an average top-1 accuracy of 27.05%, which is consistent with an
239 average set size of 3.44.

Table 2: Top-1 Accuracy of the model in predicting either the correct matching SMILES or a non-matching token. We show the performance of both the best and an ensemble of the five best checkpoints.

Model	Rxn (Top-1 Acc. %)		Mol (Top-1 Acc. %)	
	Matching	Non-Matching	Matching	Non-Matching
Random Baseline	25.05	30.54	24.75	27.68
^1H -Model	95.66	98.99	95.86	97.73
^1H -Model Ensemble of 5	96.08	99.12	95.55	97.97
^{13}C -Model	97.08	99.18	96.10	97.81
^{13}C -Model Ensemble of 5	96.34	99.23	96.30	98.03
$^1\text{H} + ^{13}\text{C}$ -Model	97.56	99.45	96.13	98.55
$^1\text{H} + ^{13}\text{C}$ -Model Ensemble of 5	98.28	99.58	95.16	99.49

240 All models demonstrate a high performance in both matching a spectrum to a molecule and detecting
 241 if a spectrum does not match any of the molecules in the set. The accuracy is notably higher
 242 when evaluated on non-matching test sets. This can potentially be attributed to the relative ease of
 243 identifying a mismatch between a spectrum and the molecules contained in the set, compared to
 244 accurately pinpointing the correct match especially if the similarity between some molecule is high.

245 The models also show high proficiency in correctly predicting the SMILES of the matching molecule.
 246 We investigate the model mistakes in this task by assigning the wrong predictions into three categories:
 247 1) "Non-Matching": the model predicts a non-matching token instead of the expected SMILES, 2)
 248 "Other Molecule in the set": the model predicts a SMILES found in the input set which does not
 249 correspond to the target SMILES and 3) "Incorrect SMILES": the model predicts a SMILES sequence
 250 that is either not found in the input set or incorrect. Results for the three ensemble model are
 251 shown in Table 3.

Table 3: Analysis of the incorrect predictions on the matching testsets.

Model	Testset	Incorrect Predictions (%)		
		Non-Matching	Other Molecule in Set	Incorrect SMILES
^1H -Model	Mol	96.81	2.56	0.64
	Rxn	10.85	88.22	0.93
^{13}C -Model	Mol	95.46	3.67	0.86
	Rxn	37.72	60.92	1.37
$^1\text{H} + ^{13}\text{C}$ -Model	Mol	99.14	0.51	0.34
	Rxn	6.69	92.20	1.11

252 Across all three models we observe a distinctly different distribution between the molecule and
 253 reaction set. For the former, most mistakes occur via the model incorrectly predicting a non-matching
 254 token. On the other hand for the reaction-testset the most common mistake consists of the model
 255 predicting a different molecule that can also be found in the set of molecules provided to the model.
 256 These differences can be attributed to the higher similarity found between molecules in the reaction
 257 sets causing the model to incorrectly assign the NMR to another molecule in the set. Reassuringly,
 258 all three models can reliably generate accurate SMILES strings from the input set. Errors arising
 259 from incorrect SMILES or SMILES that are not contained in the input set account for less than 2%
 260 of all mistakes.

261 We do not observe a significant different in between the different modalities. Models trained on
 262 ^1H , ^{13}C , and the combination perform within ~ 1 -2% of top-1 accuracy. This is points to all three
 263 modalities containing enough information to correctly match an NMR spectrum to a molecule.

264 Overall, our findings demonstrate that a transformer model can accurately assign a molecule to an
265 NMR spectrum when provided with a set of reactants and products from a reaction, achieving a high
266 level of accuracy.

267 2.5 Limitations

268 One of the key limitations of our methodological approach lies in the availability of large NMR
269 datasets. While these datasets exist, licenses for their use are often expensive and restrict machine
270 learning applications, limiting their use. Consequently, we opt to simulate NMR spectra using
271 MestreNova. While this approach is not inherently limiting, it is important to note that the resulting
272 spectra are highly coherent and consistent. Experimental spectra likely exhibit greater variability and
273 inconsistencies.

274 3 Conclusions

275 NMR spectroscopy is a very powerful tool routinely used by chemists. The analysis of spectra, or
276 rather their use for structure elucidation, remains a primarily manual task. Taking in consideration the
277 number of spectra analyzed every day in the world, it is surprising that few data-driven approaches to
278 aid in this process have been adopted so far. In this work, we explored ways to change that.

279 To this end, we presented a transformer model capable of predicting the molecular structure directly
280 from NMR spectra. We trained and optimised the transformer model to predict the molecular structure
281 from the ^1H , ^{13}C , and combined $^1\text{H}/^{13}\text{C}$ NMR spectra. We report a top-1 accuracy of 58.0%, 53.9%
282 and 67.0% for the tasks on simulated spectra, respectively. In different experiments, we observe that
283 weaknesses present in models trained on a single modality can be eliminated by combining the two
284 modalities. Erroneous model predictions are very similar to the target molecules, with an average
285 Tanimoto similarity of 0.55 for the model trained ^1H and ^{13}C spectra. This demonstrates that the
286 model predictions, even when incorrect, provide chemists with structure guesses that are close to the
287 correct compound.

288 In another task, we train models to select, among potential candidates, the molecule corresponding to
289 an NMR spectrum. We find that for all three modalities the model is able to accomplish this task with
290 a top-1 accuracy above 95%.

291 The models trained on simulated data in this work will provide a basis for fine-tuning on experimental
292 datasets, allowing the models to leverage the fundamentals learned from the simulated spectra while
293 adapting to the variability and noise found in experimental ones.

294 These advancements hold the potential to transform the analysis of NMR spectra, enabling faster
295 and more accurate identification and characterization of compounds. As a result, the integration of
296 automated NMR analysis into the workflow of high-throughput experiments promises to enhance
297 efficiency and accelerate discoveries in the field of chemistry.

298 References

- 299 [1] Qingxin Li and CongBao Kang. A Practical Perspective on the Roles of Solution NMR
300 Spectroscopy in Drug Discovery. *Molecules*, 25(13):2974, 2020.
- 301 [2] David R. Klein. *Organic Chemistry*. Wiley, 2013.
- 302 [3] Gregory M. Banik, Grace Baysinger, Prashant V. Kamat, and Norbert Pienta. *The ACS Guide to*
303 *Scholarly Communication*. American Chemical Society, 2020.
- 304 [4] Gayathri Dev Ammini, Jordan P. Hooker, Joren Van Herck, Anil Kumar, and Tanja Junkers.
305 Comprehensive high-throughput screening of photopolymerization under light intensity varia-
306 tion using inline NMR monitoring. *Polym. Chem.*, 14(22):2708–2716, 2023.
- 307 [5] Alex Krizhevsky, Ilya Sutskever, and Geoffrey E Hinton. ImageNet Classification with Deep
308 Convolutional Neural Networks. In *Advances in Neural Information Processing Systems*,
309 volume 25, 2012.

- 310 [6] Ashish Vaswani, Noam Shazeer, Niki Parmar, Jakob Uszkoreit, Llion Jones, Aidan N. Gomez,
311 Lukasz Kaiser, and Illia Polosukhin. Attention Is All You Need, 2017. arXiv:1706.03762.
- 312 [7] Philippe Schwaller, Teodoro Laino, Théophile Gaudin, Peter Bolgar, Christopher A. Hunter,
313 Costas Bekas, and Alpha A. Lee. Molecular Transformer: A Model for Uncertainty-Calibrated
314 Chemical Reaction Prediction. *ACS Cent. Sci.*, 5(9):1572–1583, 2019.
- 315 [8] Zhichao Liu, Ruth A. Roberts, Madhu Lal-Nag, Xi Chen, Ruili Huang, and Weida Tong. AI-
316 based language models powering drug discovery and development. *Drug Discovery Today*,
317 26(11):2593–2607, 2021.
- 318 [9] Andres M. Bran, Sam Cox, Andrew D. White, and Philippe Schwaller. ChemCrow: Augmenting
319 large-language models with chemistry tools, 2023. arXiv:2304.05376.
- 320 [10] Melodie Christensen, Lars P. E. Yunker, Parisa Shiri, Tara Zepel, Paloma L. Prieto, Shad
321 Grunert, Finn Bork, and Jason E. Hein. Automation isn’t automatic. *Chemical Science*,
322 12(47):15473–15490, 2021.
- 323 [11] Milad Abolhasani and Eugenia Kumacheva. The rise of self-driving labs in chemical and
324 materials sciences. *Nat. Synth*, 2(6):483–492, 2023.
- 325 [12] Steven M. Mennen, Carolina Alhambra, C. Liana Allen, Mario Barberis, Simon Berritt,
326 Thomas A. Brandt, Andrew D. Campbell, Jesús Castañón, Alan H. Cherney, Melodie Chris-
327 tensen, David B. Damon, J. Eugenio de Diego, Susana García-Cerrada, Pablo García-Losada,
328 Rubén Haro, Jacob Janey, David C. Leitch, Ling Li, Fangfang Liu, Paul C. Lobben, David W. C.
329 MacMillan, Javier Magano, Emma McInturff, Sebastien Monfette, Ronald J. Post, Danielle
330 Schultz, Barbara J. Sitter, Jason M. Stevens, Iulia I. Strambeanu, Jack Twilton, Ke Wang, and
331 Matthew A. Zajac. The Evolution of High-Throughput Experimentation in Pharmaceutical
332 Development and Perspectives on the Future. *Org. Process Res. Dev.*, 23(6):1213–1242, 2019.
- 333 [13] Alexander Buitrago Santanilla, Erik L. Regalado, Tony Pereira, Michael Shevlin, Kevin Bate-
334 man, Louis-Charles Campeau, Jonathan Schneeweis, Simon Berritt, Zhi-Cai Shi, Philippe
335 Nantermet, Yong Liu, Roy Helmy, Christopher J. Welch, Petr Vachal, Ian W. Davies, Tim
336 Cernak, and Spencer D. Dreher. Nanomole-scale high-throughput chemistry for the synthesis
337 of complex molecules. *Science*, 347(6217):49–53, 2015.
- 338 [14] Damith Perera, Joseph W. Tucker, Shalini Brahmabhatt, Christopher J. Helal, Ashley Chong,
339 William Farrell, Paul Richardson, and Neal W. Sach. A platform for automated nanomole-scale
340 reaction screening and micromole-scale synthesis in flow. *Science*, 359(6374):429–434, 2018.
- 341 [15] Michael Shevlin. Practical High-Throughput Experimentation for Chemists. *ACS Med. Chem.*
342 *Lett.*, 8(6):601–607, 2017.
- 343 [16] Babak Mahjour, Rui Zhang, Yuning Shen, Andrew McGrath, Ruheng Zhao, Osama G. Mo-
344 hamed, Yingfu Lin, Zirong Zhang, James L. Douthwaite, Ashootosh Tripathi, and Tim Cernak.
345 Rapid planning and analysis of high-throughput experiment arrays for reaction discovery. *Nat*
346 *Commun*, 14(1):3924, 2023.
- 347 [17] Adam Cook, Roxanne Clément, and Stephen G. Newman. Reaction screening in multi-
348 well plates: high-throughput optimization of a Buchwald–Hartwig amination. *Nat Protoc.*
349 16(2):1152–1169, 2021.
- 350 [18] MestreLab, MNova. <https://mestrelab.com/software/mnova/> (Accessed July 24,
351 2023).
- 352 [19] ACD Labs, NMR Workbook Suite. [https://www.acdlabs.com/products/
353 spectrus-platform/nmr-workbook-suite/](https://www.acdlabs.com/products/spectrus-platform/nmr-workbook-suite/) (Accessed July 24, 2023).
- 354 [20] Zhaorui Huang, Michael S. Chen, Cristian P. Woroch, Thomas E. Markland, and Matthew W.
355 Kanan. A framework for automated structure elucidation from routine NMR spectra. *Chem.*
356 *Sci.*, 12(46):15329–15338, 2021.
- 357 [21] Eric Jonas. Deep imitation learning for molecular inverse problems. In *Advances in Neural*
358 *Information Processing Systems*, volume 32, 2019.

- 359 [22] Weiwei Wei, Yuxuan Liao, Yufei Wang, Shaoqi Wang, Wen Du, Hongmei Lu, Bo Kong, Huawu
360 Yang, and Zhimin Zhang. Deep Learning-Based Method for Compound Identification in NMR
361 Spectra of Mixtures. *Molecules*, 27(12):3653, 2022.
- 362 [23] Iván Cortés, Cristina Cuadrado, Antonio Hernández Daranas, and Ariel M. Sarotti. Machine
363 learning in computational NMR-aided structural elucidation. *Frontiers in Natural Products*, 2,
364 2023.
- 365 [24] Jinzhe Zhang, Kei Terayama, Masato Sumita, Kazuki Yoshizoe, Kengo Ito, Jun Kikuchi, and
366 Koji Tsuda. NMR-TS: de novo molecule identification from NMR spectra. *Science and
367 Technology of Advanced Materials*, 21(1):552–561, 2020.
- 368 [25] NextMove Software, Pistachio. <https://www.nextmovesoftware.com/pistachio.html>
369 (Accessed July 24, 2023).
- 370 [26] Marvin Alberts, Teodoro Laino, and Alain C. Vaucher. Leveraging Infrared Spectroscopy for
371 Automated Structure Elucidation, 2023. DOI: 10.26434/chemrxiv-2023-5v27f.
- 372 [27] David Weininger. SMILES, a chemical language and information system. 1. Introduction to
373 methodology and encoding rules. *J. Chem. Inf. Comput. Sci.*, 28(1):31–36, 1988.
- 374 [28] David Weininger, Arthur Weininger, and Joseph L. Weininger. SMILES. 2. Algorithm for
375 generation of unique SMILES notation. *J. Chem. Inf. Comput. Sci.*, 29(2):97–101, May 1989.
- 376 [29] Dávid Bajusz, Anita Rácz, and Károly Héberger. Why is Tanimoto index an appropriate choice
377 for fingerprint-based similarity calculations? *Journal of Cheminformatics*, 7(1):20, 2015.
- 378 [30] David Rogers and Mathew Hahn. Extended-Connectivity Fingerprints. *J. Chem. Inf. Model.*,
379 50(5):742–754, 2010.
- 380 [31] OpenNMT-py: Open-Source Neural Machine Translation, 2017. [https://github.com/
381 OpenNMT/OpenNMT-py](https://github.com/OpenNMT/OpenNMT-py) (Accessed July 24, 2023).
- 382 [32] Guillaume Klein, Yoon Kim, Yuntian Deng, Jean Senellart, and Alexander M. Rush. OpenNMT:
383 Open-Source Toolkit for Neural Machine Translation, 2017. arXiv:1701.02810.
- 384 [33] RDKit. <https://www.rdkit.org/> (Accessed July 24, 2023).
- 385 [34] Daylight: SMARTS Examples. [https://www.daylight.com/dayhtml_tutorials/
386 languages/smarts/smarts_examples.html](https://www.daylight.com/dayhtml_tutorials/languages/smarts/smarts_examples.html) (Accessed April 20, 2023).

387 Appendix

388 A Methods

389 A.1 Synthetic Data

390 Before generating spectra, 1,029,381 reactions were sampled from the Pistachio patent dataset [25]. A
391 set of molecules was assembled from the precursors and products of these reactions. Molecules were
392 filtered out if they contain atoms other than carbon, hydrogen, oxygen, nitrogen, sulfur, phosphorous
393 and the halogens. In addition, all molecules with a heavy atom count outside the range of 5–35,
394 charged molecules or containing isotope information were filtered out.

395 From this set, 1,120,390 ^1H and 1,943,950 ^{13}C NMR spectra were generated using MestreNova.
396 Standard simulation settings were used for ^1H NMRs. For ^{13}C NMRs, ^1H and ^{19}F decoupled spectra
397 were generated. For ^{13}C NMR, the position of all peaks was recorded. On the other hand ^1H
398 NMR were further processed. First peak-picking was applied, followed by the autointegration and
399 automultiplet assignment. All three processing steps were carried out using built-in MestreNova
400 functions with standard settings. For each peak in an ^1H NMR, the range of the peak, its centroid, the
401 number of hydrogen atoms and the multiplet was recorded.

402 A.2 Model

403 We base our model architecture on the Molecular Transformer [7]. The model takes the formatted
404 NMR spectrum with the chemical formula as input, and outputs a molecular structure encoded as
405 SMILES. This can be formulated as a translation task from the spectrum to the molecular structure.
406 The model is a vanilla transformer as implemented in the OpenNMT-py library [31, 32] with the
407 following hyperparameters deviating:

```
408 word_vec_size: 512  
409 hidden_size: 512  
410 layers: 4  
411 batch_size: 4096
```

412 All models are trained for 350k steps amounting to approximately 35h on a A100 GPU.

413 A.3 Tokenization

414 To tokenize ^1H NMR peaks, we proceed as follows. The position of the peak is rounded to the second
415 decimal point, the type of multiplet (singlet, doublet, triplet, etc.) and the number of hydrogens are
416 appended as second and third token respectively. All peaks are separated with a separating token
417 (“|”). As an example a singlet at 1.239 ppm with an integral of 3 would become “1.24 s 3H |”,
418 with tokens separated by whitespaces. A string of the ^1H NMR spectrum is built accordingly by
419 concatenating the peaks starting with the lowest ppm and ending at the highest one. In addition, a
420 prefix token is used to differentiate ^1H from ^{13}C NMR spectra. As an example an ^1H NMR with two
421 peaks would be formatted as follows: “ $^1\text{HNMR}$ 1.24 t 3H | 1.89 q 3H |”.

422 ^{13}C NMR are formatted according to a simpler scheme. As the multiplet type and integration is not
423 relevant for this type of spectrum the position of the peaks are rounded to one decimal point and
424 tokenized accordingly. To illustrate this, a typical NMR spectrum is tokenized as follows: “ $^{13}\text{CNMR}$
425 12.1 27.8 63.5”.

426 In addition to the spectra, the model is provided the chemical formula in addition to the NMR
427 spectrum. The formula is calculated using RDKit [33] and prepended to the spectrum.

428 When both ^1H and ^{13}C NMR are used, the tokenized string consists first of the chemical formula,
429 followed by the ^1H NMR spectrum and finally the ^{13}C NMR. To have the ^1H and ^{13}C NMR share
430 the same token space, the ppm values of the ^{13}C NMR peaks are divided by 10.

431 A.4 Data augmentation

432 The spectra are augmented using jitter augmentation as used previously by Jonas et. al. [21]. This
433 involves adding a random distortion sampled from a range of 0.5 ppm for ^1H NMR and 5 ppm for

434 ¹³C NMR. The random noise is added to each of the peaks in the spectra. In total, two augmented
 435 spectra are produced for each original one.

436 B Functional group definitions

437 Functional groups are defined in SMARTS as shown in Table 4. Using these SMARTS
 438 and RDKit the presence of a certain function group is determined by invoking <RDKit
 439 molecule>.GetSubstrucMatches(<RDKit molecule from SMARTS pattern>)

Table 4: Functional group definitions used.

	Definition
Alcohol	[OX2H] [CX4; !\$ (C ([OX2H]) [O,S,#7,#15])]
Carboxylic Acid	[CX3] (=O) [OX2H1]
Ester	[#6] [CX3] (=O) [OX2H0] [#6]
Ether	[OD2] ([#6]) [#6]
Aldehyde	[CX3H1] (=O) [#6]
Ketone	[#6] [CX3] (=O) [#6]
Alkene	[CX3]=[CX3]
Alkyne	[\$ ([CX2]#C)]
Benzene	c1ccccc1
Primary Amine	[NX3;H2; !\$ (NC=[!#6]); !\$ (NC#[!#6])] [#6]
Secondary Amine	[NH1,nH1])
Tertiary Amine	[NHO,nH0])
Amide	[NX3] [CX3] (= [OX1]) [#6]
Cyano	[NX1]# [CX2]
Fluorine	[#6] [F]
Chlorine	[#6] [Cl]
Iodine	[#6] [I]
Bromine	[#6] [Br]
Sulfonamide	[#16X4] ([NX3]) (= [OX1]) (= [OX1]) [#6]
Sulfone	[#16X4] (= [OX1]) (= [OX1]) ([#6]) [#6]
Sulfide	[#16X2H0]
Phosphoric Acid [†]	[\$ (P (= [OX1]) (\$ ([OX2H]), \$ ([OX1-]), \$ ([OX2]P))) (\$ ([OX2H]), \$ ([OX1-]), \$ ([OX2]P)) (\$ ([OX2H]), \$ ([OX1-]), \$ ([OX2]P)), \$ ([P+] ([OX1-]) (\$ ([OX2H]), \$ ([OX1-]), \$ ([OX2]P))) (\$ ([OX2H]), \$ ([OX1-]), \$ ([OX2]P)) (\$ ([OX2H]), \$ ([OX1-]), \$ ([OX2]P)))]

[†] Adapted from [34]

440 **C Performance on molecules containing specific functional groups**

441 In Tables 5, 6, and 7, the accuracy of the model solely trained on ^1H , ^{13}C , and combined $^1\text{H}/^{13}\text{C}$
 442 NMR data, respectively, is shown depending on the presence of specific functional groups in the
 443 target molecule. “Count” represents the number of molecules with this functional group in the test set.
 444 Additionally, the average heavy atom count (“Avg. HAC” in the table) is calculated to rule out bias.

Table 5: The model trained on ^1H NMR spectra’s ability to predict the correct molecular structure based on if a specific functional group is present in the target molecule.

	Count	Avg. HAC	Top-1%	Top-5%	Top-10%
Phosphoric Acid	76	27.09	31.58	47.37	48.68
Alkene	12727	22.55	46.94	66.87	70.46
Cyano	7691	23.58	53.54	71.92	75.83
Alkyne	2071	23.39	54.23	71.61	74.89
Alcohol	17214	22.86	54.23	74.83	78.49
Sulfide	15214	23.85	55.06	73.41	77.06
Primary Amine	12504	21.30	55.42	75.99	79.57
Amide	31834	26.10	56.13	74.26	77.77
Chlorine	23685	23.59	56.42	75.31	78.95
Tertiary Amine	83118	24.01	56.74	74.85	78.30
Carboxylic Acid	13838	23.26	56.79	77.03	80.60
Ketone	8100	22.35	56.91	73.10	76.35
Secondary Amine	56201	24.50	56.96	75.16	78.65
Fluorine	30166	25.16	57.70	75.59	78.97
Ether	34926	24.98	58.75	76.93	80.16
Sulfone	2428	26.03	58.86	75.41	78.46
Benzene	86972	24.08	58.86	76.92	80.18
Sulfonamide	5758	26.44	59.48	76.55	79.63
Ester	16344	23.20	59.50	79.08	82.13
Aldehyde	2208	19.09	60.19	79.71	83.02
Bromine	9687	20.11	60.48	80.21	83.47
Iodine	1728	19.93	62.21	82.52	85.30

Table 6: The model trained on ^{13}C NMR spectra's ability to predict the correct molecular structure based on if a specific functional group is present in the target molecule.

	Count	Avg. HAC	Top-1%	Top-5%	Top-10%
Phosphoric Acid	142	26.54	36.62	55.63	59.86
Alkene	21149	23.09	40.65	60.35	64.87
Alcohol	21781	23.11	48.25	69.14	74.11
Sulfide	26917	23.90	50.54	69.80	74.08
Primary Amine	22672	21.39	51.14	72.07	76.61
Amide	51806	26.33	51.29	69.90	74.21
Cyano	13327	23.34	51.30	70.18	74.57
Chlorine	40757	23.39	51.43	71.69	76.30
Secondary Amine	85969	24.94	51.97	71.35	75.62
Tertiary Amine	146144	24.10	52.21	71.32	75.66
Fluorine	49707	25.00	52.33	72.09	76.49
Carboxylic Acid	18879	23.21	54.47	75.34	79.46
Iodine	3193	19.40	54.56	76.20	80.74
Sulfone	4928	25.85	54.61	71.25	75.59
Benzene	149174	24.31	54.79	73.83	77.95
Alkyne	3700	23.31	54.89	73.14	76.89
Bromine	17680	19.99	55.71	76.84	81.46
Sulfonamide	9319	26.70	55.77	73.00	76.97
Ketone	14910	22.41	56.32	73.66	77.94
Ether	65246	25.10	56.60	75.00	78.97
Aldehyde	4452	19.25	57.46	78.23	82.88
Ester	33632	23.47	58.11	78.01	81.80

Table 7: The model trained on both ^1H and ^{13}C NMR spectra's ability to predict the correct molecular structure based on if a specific functional group is present in the target molecule.

	Count	Avg. HAC	Top-1%	Top-5%	Top-10%
Phosphoric Acid	71	25.82	38.03	50.70	54.93
Alkene	12799	22.36	54.68	74.48	77.40
Alcohol	16967	22.77	62.32	82.14	85.04
Primary Amine	12378	21.36	63.94	83.16	85.85
Sulfide	15219	24.17	64.02	80.92	83.68
Amide	32013	26.12	64.90	82.31	85.11
Chlorine	23849	23.58	65.57	82.79	85.53
Secondary Amine	56290	24.50	65.67	82.79	85.55
Cyano	7767	23.61	65.91	82.17	84.97
Fluorine	30724	25.09	66.00	82.98	85.66
Sulfone	2537	26.08	66.30	81.75	84.15
Tertiary Amine	83173	24.01	66.31	82.98	85.59
Carboxylic Acid	13719	23.30	66.80	85.41	87.82
Alkyne	2070	23.49	66.86	83.24	85.89
Ketone	8241	22.29	67.10	82.55	85.01
Ester	16499	23.25	67.66	85.24	87.50
Benzene	87374	24.05	67.85	84.40	86.86
Ether	34823	24.86	67.87	84.35	86.75
Sulfonamide	5663	26.58	68.20	83.68	86.39
Iodine	1705	19.88	68.68	85.34	87.21
Bromine	9838	20.19	69.66	86.91	89.04
Aldehyde	2152	19.11	70.77	87.04	89.22

445 **D Tanimoto Similarity Distribution**

446 In Figure 5 the Tanimoto similarity distribution for all three models is illustrated. The distribution
447 shows a peak around 0.55 for all three models.

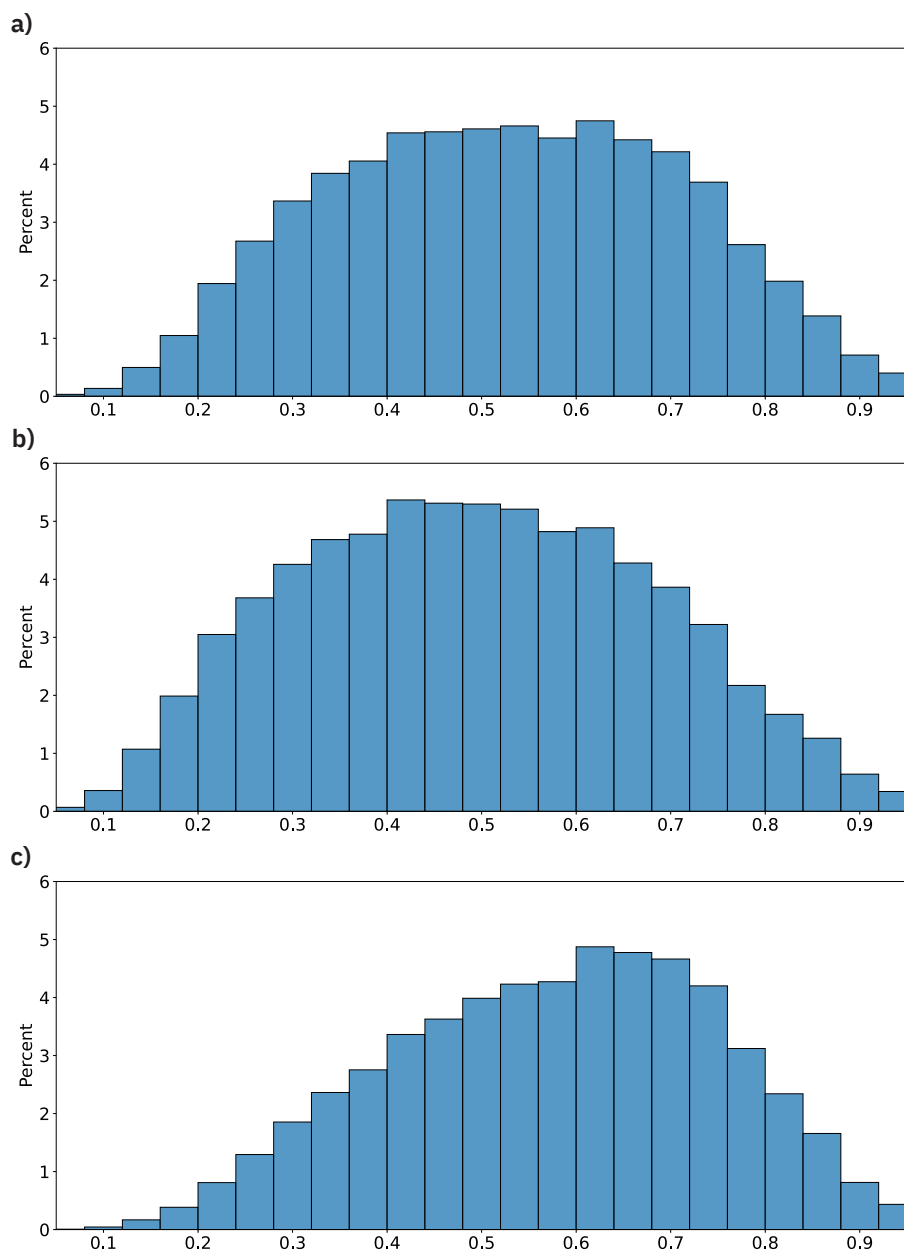


Figure 5: The Tanimoto distribution of three models: a) ^1H NMR, b) ^{13}C NMR, c) $^1\text{H}+^{13}\text{C}$ NMR. All correct molecules were excluded.